Early scaffold strut coverage in ultra-high molecular weight amorphous PLLA sirolimus-eluting bioresorbable scaffolds: impact of strut thickness assessed in normal porcine coronary arteries

Paweł Gąsior[1,2], Yanping Cheng[1], Marco Ferrone[1,3], Jenn C. McGregor[1], Gerard B. Conditt[1], Juan F. Granada[1], Grzegorz L. Kaluza[1]

[1]CRF-Skirball Center for Innovation, Orangeburg, NY, USA
[2]Division of Cardiology and Structural Heart Diseases, Medical University of Silesia, Katowice, Poland
[3]Federico II University, Naples, Italy

Adv Interv Cardiol 2020; 16, 1 (59): 102–106
DOI: https://doi.org/10.5114/aic.2020.93917

Introduction

The first FDA-approved bioresorbable scaffold (BRS) Absorb BVS (Abbott Vascular, USA) demonstrated a higher rate of scaffold thrombosis when compared to current-generation metallic drug-eluting stents (DES) [1]. It is believed that the bulky strut thickness of 156 µm, exceeding nearly twice that of contemporary metallic DES, is responsible for the higher thrombotic potential of this technology [2].

The speed and quality of stent/scaffold strut coverage by tissue are strongly impacted by strut thickness and shape, which influence shear stress and blood flow dynamics, affecting platelet accumulation and endothelial cell growth [3–5]. Regardless of strut height, non-streamlined scaffold struts influence blood flow recirculation and low flow shear rates and prolong particulate residence time [6]. Low endothelial shear stress influences endothelialization rates, and taller strut height induces an environment of procoagulant and proinflammatory elements, which can lead to a greater quantity of thrombus and also accelerate turnover of endothelial cells, making reendothelialization more difficult [7, 8]. Preclinical studies demonstrated that strut thickness influences thrombogenicity, with struts that are < 100 µm having smaller thrombi than struts that are > 100 µm [9]. Therefore, the reduction in strut thickness resulting in improved vascular healing with neointimal strut coverage is a crucial concept in developing new BRS.

In this study we aimed to evaluate the short-term healing response using optical coherence tomography (OCT) following implantation of a new-generation sirolimus-eluting amorphous PLLA-based BRS (Amaranth Medical, USA) with ultra-thin strut (98-µm, AMA-98) and thin strut (115-µm, AMA-115) thickness in porcine coronary arteries.

Material and methods

Device description

Scaffolds used in this study have almost identical ring design and different strut thicknesses: the ultra-thin strut AMA-98, with strut thickness of 98 µm; and the thin strut AMA-115, with strut thickness of 115 µm. The only difference between the 2 versions is a slightly increased surface area coverage at rated burst pressure in AMA-98 when compared to AMA-115 (respectively: 22% vs. 21% for 3.0 mm scaffolds). Both scaffolds were manufactured by the same company (Amaranth Medical, USA) using an ultra-high molecular weight bioresorbable polylactide-based polymer. Devices are coated with a matrix consisting of a 1 : 1 polymer : drug ratio of sirolimus plus Poly D-Lactide polymer and with a sirolimus dose density of ~96 µg/cm^2. The core AMA-BRS technology was described in detail previously [10–12]. Both devices underwent extensive preclinical testing and are currently evaluated in the first-in-men clinical trials.

Study design

The Institutional Animal Care and Use Committee approved all studies, and all animals received care in ac-

Corresponding author:
Grzegorz L. Kaluza MD, PhD, CRF-Skirball Center for Innovation, Orangeburg, NY, USA, phone: +18455803082, e-mail: gkaluza@crf.org
Received: 20.11.2019, **accepted:** 2.12.2019.

cordance with the Guide to Care and Use of Laboratory Animals. All animals underwent endotracheal intubation and were maintained on continuous inhalation of 1–3% isoflurane. Anticoagulation with heparin was achieved during the procedure (500–5,000 U) to maintain an activated clotting time (ACT) ≥ 250 s. In this study either AMA-95 (n = 12, size 2.5, 3.0, 3.5 × 18 mm) or AMA-115 (n = 15, size 2.5, 3.0, 3.5 × 18 mm) were implanted targeting a stent-to-artery ratio of 1.1 : 1 under intravascular ultrasound guidance in 26 porcine coronary arteries of 16 Yucatan mini swine. *In vivo* structural integrity and recoil, as well as strut-vessel wall interactions, were evaluated longitudinally at 14 and 28 days using optical coherence tomography.

Optical coherence tomography imaging

OCT images were recorded at post-implantation day 0 and at follow-ups using the ILUMIEN PCI Optimization System (St. Jude Medical, USA) following a previously published protocol [8] and the cross-sectional morphometry parameters were measured with commercial software (ILUMIEN OPTIS, St. Jude Medical, USA) as previously described [5–7] at 2-mm axial intervals. The following cross-sectional morphometry parameters were measured and calculated as previous described [10]: lumen area, inner and outer scaffold area, percentage area of stenosis. Absolute late recoil was measured as the mean scaffold area at baseline (post-implant) minus the mean scaffold area at follow-up. Relative late recoil (normalized to scaffold size) was calculated as: [(absolute late recoil)/baseline mean scaffold area] × 100 [11].

In order to determine the presence of strut tissue coverage in AMA-BRS, the thickness of the endoluminal bright border in 300 frames from 10 scaffolds struts located close to the 12 o'clock position was measured. The threshold for coverage was 30 µm, which corresponds to the average interobserver measurement of the endoluminal bright border of the strut [12]. Evaluated struts were assigned to 1 of the 3 following categories: covered with complete inter-strut neointima (embedded), covered without complete inter-strut neointima (protruding covered) and struts without evidence of coverage (uncovered).

Statistical analysis

Statistical analysis were performed using SAS statistical software (version 9.4; SAS Institute Inc. NC). Continuous variables were expressed as mean ± SD with the median and interquartile range used for variables with non-normal distributions. A mixed model compared differences between the 2 treatments (AMA-98 vs. AMA-115) while accounting for dependent observation over time. Furthermore, this model contained a random effect with compound symmetric covariance structure to account for multiple scaffolds implanted in the same pig. The device, time, and interaction between time and device were modeled as fixed effects. Scheffe's post hoc test was applied to compare differences between time points and differences between treatments at each time point. A nonparametric test was used for those dependent variables with non-normal distributions to account for multiple scaffolds implanted in the same pig. All tests were 2-tailed with a type I error held at 0.05.

Results and discussion

On day 0, post-implant OCT indicated that all scaffold struts were fully apposed to the vessel wall with no strut malapposition observed in any of the implanted vessels. No post-dilation was performed. In total, 536 cross-sections and 4223 struts were evaluated to sequentially assess In vivo structural integrity and recoil, as well as strut-vessel wall interactions and short-term strut healing response at 14 and 28 days (Figure 1). The percentage of embedded struts was significantly higher at 14 days in the AMA-98 group (AMA-98 = 97.7% (95.2, 89.1) vs. AMA-115 = 71.0% (69.5, 92.2), p = 0.007). Conversely, the presence of protruding covered struts was more commonly seen in AMA-115 at 14 days (AMA-98 = 1.7% (1.7, 4.8) vs. AMA-115 = 17.3% (7.6, 17.3), p = 0.012). There was no difference in the uncovered struts between AMA-98 and AMA-115 at 14 days. At the 28-day follow-up no statistical difference in coverage was observed between tested devices. There was no difference in the reference lumen area between AMA-98 and AMA-115 groups. However, abluminal scaffold area was smaller immediately after implantation and during 14 days of follow-up in the AMA-98 group compared to AMA-115. Percent area stenosis was similar in both scaffolds at 14- and 28-day follow-up. The results of OCT morphometric analysis are summarized in Table I.

The impact of strut thickness on early vascular healing and neointimal proliferation has been well described. Studies of coronary flow dynamics suggest that strut thickness induces laminar flow disturbances around the struts, potentially increasing thrombogenicity of the device [8]. Early BRSs have achieved an acute biomechanical performance comparable to metallic stents but at the expense of greater strut thickness. Novel PLLA formulations promise to improve biomechanical properties of current generation BRS devices. Our previous studies demonstrated higher overexpansion capabilities and dramatic improvement in resistance to fracture under static and dynamic conditions with ultrahigh molecular weight amorphous polymers [10, 12, 13].

The objective of this study was to evaluate the impact of strut thickness on early vascular healing using OCT over the first month after implant, when the scaffold interactions with blood flow matter more than the artery wall's response to injury. Our results demonstrated that AMA-98 displayed superior strut coverage in the early phase of vessel healing compared to AMA-115. At 14 days the percentage of embedded struts was significant-

ly higher in the AMA-98 group. Conversely the rate of protruding covered struts at 14 days was greater in the AMA-115 group. Interestingly, the difference occurred despite the fairly modest difference in strut thickness, corroborating earlier computer modeling and *in vivo* research on this topic [9]. There was no difference in the uncovered struts rate between the two tested scaffolds at any timepoint. Also, the more favorable strut coverage with thinner struts did not occur at the expense of higher late recoil, which was equivalent in both devices at 1 month. As expected, the neointimal proliferation expressed by percent area stenosis was low and similar in both groups.

The present study has some limitations that are important to discuss. The study was performed in healthy coronary arteries in a swine model. All scaffolds were implanted in the main coronary artery segments, avoiding large side branches (> 2.0 mm), and the number of implants at each time point was too small to draw any definite conclusion. Our findings cannot predict their clinical performance among patients with atherosclerotic burden.

Conclusions

Our data demonstrate that the ultra-thin strut AMA-98 featured more favorable strut coverage charac-

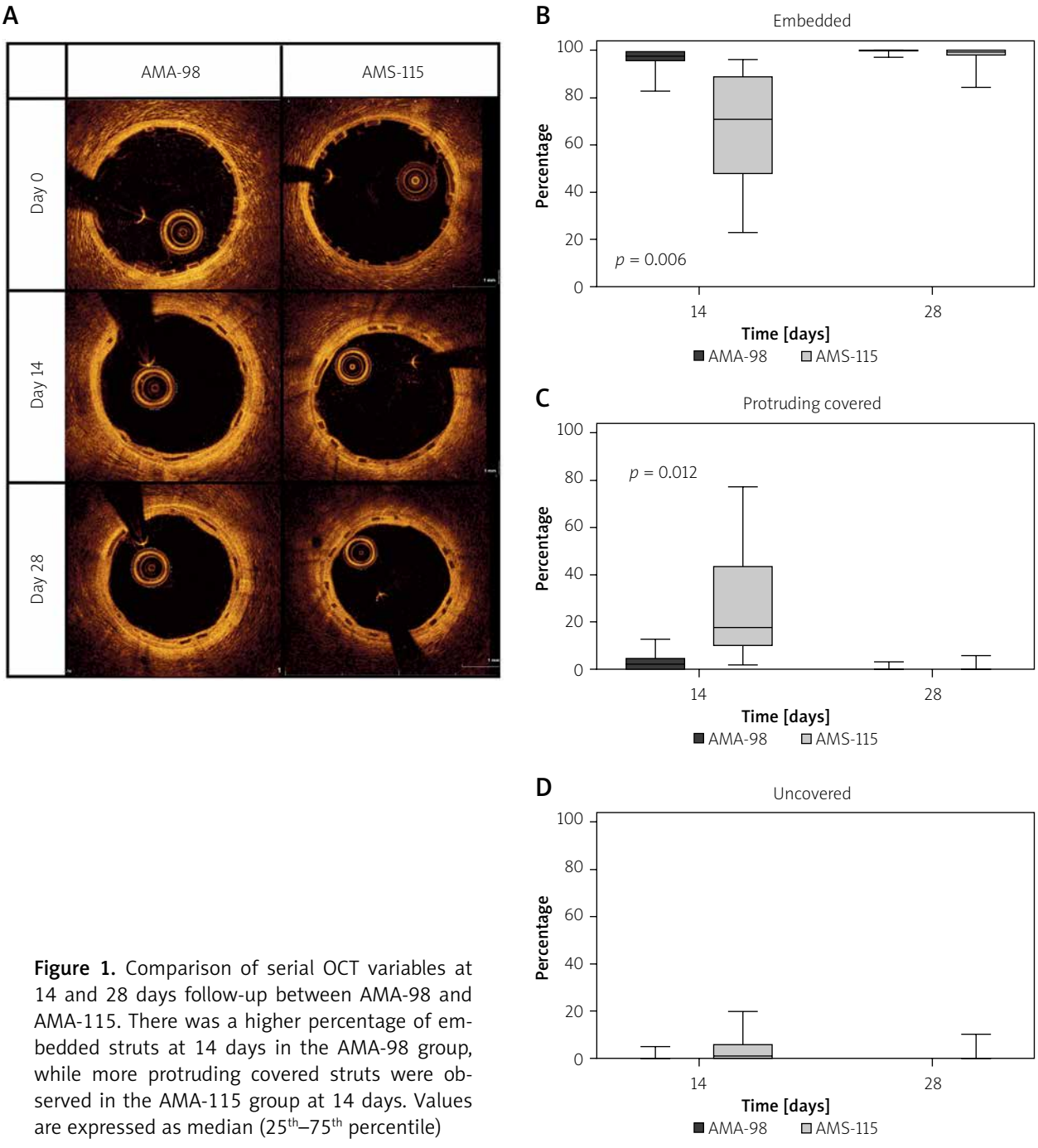

Figure 1. Comparison of serial OCT variables at 14 and 28 days follow-up between AMA-98 and AMA-115. There was a higher percentage of embedded struts at 14 days in the AMA-98 group, while more protruding covered struts were observed in the AMA-115 group at 14 days. Values are expressed as median (25^{th}–75^{th} percentile)

Table I. Morphometric OCT data

Parameter	14 days	28 days	*P*-value*
Lumen area [mm²]:			
AMA-95	6.12 ±0.63	5.12 ±0.62#	0.001
AMA-115	6.97 ±0.90	6.14 ±0.95#	
P-value†	0.007	0.076	
Endoluminal scaffold area [mm²]:			
AMA-95	6.78 ±0.58	6.42 ±0.51	0.102
AMA-115	7.64 ±0.96	7.47 ±0.99	
P-value†	0.007	0.120	
Abluminal scaffold area [mm²]:			
AMA-95	7.73 ±0.63	7.32 ±0.56#	0.098
AMA-115	8.71 ±1.00	7.99 ±1.44#	
P-value†	0.005	0.353	
Area stenosis (%):			
AMA-95	9.87 ±2.80	20.4 ±4.8#	< 0.001
AMA-115	8.78 ±1.66	17.96 ±6.43#	
P-value†	0.547	0.436	
Absolute scaffold recoil [mm²]:			
AMA-95	–0.35 (–0.57, –0.10)	0.02 (–0.13, 0.28)#	< 0.001
AMA-115	–0.10 (–0.43, 0.12)	0.07 (–0.07, 0.32)#	
P-value†	0.335	0.795	
Percent scaffold recoil (%):			
AMA-95	–5.54 (–9.32, –1.85)	0.22 (–2.11, 4.20)	< 0.001
AMA-115	1.46 (–6.11, 1.73)	1.02 (–0.90, 4.49)#	
P-value†	0.118	0.872	

*Mean ± SD. #p < 0.05 vs. 1 month. *P-value for overall change over time. †P-value for AMA BRS vs. Absorb BVS at each time point.*

teristics at early follow-up in normal porcine coronary arteries compared to the thin strut AMA-115 with similar ring design, at no expense to acute or late recoil. Interestingly, the semiquantitative differences were significant even though the strut thickness between the 2 devices differed only by 17 µm.

Acknowledgments

This study was funded by Amaranth Medical, Inc.

Conflict of interest

Juan F. Granada was a scientific advisor of Amaranth Medical, Inc. Other authors declare no conflict of interest.

References

1. Kereiakes DJ, Ellis SG, Metzger C, et al. 3-year clinical outcomes with everolimus-eluting bioresorbable coronary scaffolds: the ABSORB III trial. J Am Coll Cardiol 2017; 70: 2852-62.
2. Otsuka F, Cheng Q, Yahagi K, et al. Acute thrombogenicity of a durable polymer everolimus-eluting stent relative to contemporary drug-eluting stents with biodegradable polymer coatings assessed ex vivo in a swine shunt model. JACC Cardiovasc Interv 2015; 8: 1248-60.
3. Simon C, Palmaz, JC, Sprague EA. Influence of topography on endothelialization of stents: clues for new designs. J Long Term Eff Med Implants 2000; 10: 143-51.
4. LaDisa JF Jr, Olson LE, Douglas HA, et al. Alterations in regional vascular geometry produced by theoretical stent implantation influence distributions of wall shear stress: analysis of a curved

coronary artery using 3D computational fluid dynamics modeling. Biomed Eng Online 2006; 5: 40.
5. Richter Y, Edelman ER. Cardiology is flow. Circulation 2006; 113: 2679-82.
6. Sanchez OD, Yahagi K, Byrne RA, et al. Pathological aspects of bioresorbable stent implantation. EuroIntervention 2015; 11 Suppl V: V159-65.
7. Tricot O, Mallat Z, Heymes C, et al. Relation between endothelial cell apoptosis and blood flow direction in human atherosclerotic plaques. Circulation 2000; 101: 2450-3.
8. Tenekecioglu E, Torii R, Bourantas C, et al. Preclinical assessment of the endothelial shear stress in porcine-based models following implantation of two different bioresorbable scaffolds: effect of scaffold design on the local haemodynamic micro-environment. EuroIntervention 2016; 12: 1296.
9. Kolandaivelu K, Swaminathan R, Gibson WJ, et al. Stent thrombogenicity early in high-risk interventional settings is driven by stent design and deployment and protected by polymer-drug coatings. Circulation 2011; 123: 1400-9.
10. Cheng Y, Gasior P, Shibuya M, et al. Comparative characterization of biomechanical behavior and healing profile of a novel ultra-high-molecular-weight amorphous poly-l-lactic acid sirolimus-eluting bioresorbable coronary scaffold. Circ Cardiovasc Interv 2016; 12: 1164-73.
11. Onuma Y, Serruys PW, Gomez J, et al. Comparison of in vivo acute stent recoil between the bioresorbable everolimus-eluting coronary scaffolds (revision 1.0 and 1.1) and the metallic everolimus-eluting stent. Catheter Cardiovasc Interv 2011; 78: 3-12.
12. Cheng Y, Gasior P, Xia JG, et al. Comparative biomechanical behavior and healing profile of a novel thinned-wall ultrahigh molecular weight amorphous poly-l-lactic acid sirolimus-eluting bioresorbable coronary scaffold. Circ Cardiovasc Interv 2017; 10. pii: e005116.
13. Gasior P, Cheng Y, Estrada EA, et al. Novel ultrahigh molecular weight amorphous PLLA bioresorbable coronary scaffold upsized up to 0.8 mm beyond nominal diameter: an OCT and histopathology study in porcine coronary artery model. Catheter Cardiovasc Interv 2018; 91: 378-86.